Environ Model Assess
DOI 10.1007/s10666-015-9459-1

Sediment Diagenesis Module for CE-QUAL-W2 Part 2: Numerical Formulation

Shwet Prakash[1] · **Jerry A. Vandenberg**[2] · **Edward M. Buchak**[1]

Received: 27 November 2014 / Accepted: 24 March 2015

Abstract Pit lakes are used worldwide as part of closure schemes for mining operations. Pit lakes have also been proposed in the Athabasca Oil Sands Region of Canada where bitumen is close enough to the surface to be recovered using conventional surface mining and chemical extraction procedures. Many of the pit lakes are designed to cap tailings with a substantial water layer. The pore water in tailings will contain various amounts of labile and refractory organic compounds, nutrients, trace metals, and ion concentrations that, ultimately, will be released to the water cap as the tailings consolidate. In addition to advective release of constituents from the tailings pore water, chemical reactions, more specifically, diagenetic processes, within the tailings will result in changes to the redox state, speciation, and phase of several chemicals. A module that quantifies diagenetic processes has been developed for the 2-dimensional hydrodynamic and water quality model, CE-QUAL-W2. The module includes processes such as biogenic gas production (build up and release of methane, hydrogen sulfide, and ammonia); physical release of bubbles through the water column; unconsolidated sediment resuspension during bubble ebullition; and dynamic oxygen consumption at the sediment–water interface and in the water column from bubbles. This paper presents the numerical framework used to develop the diagenesis module and the chemical basis for the algorithms.

Keywords Athabasca oil sands · End pit lakes · Mature fine tailings · Methane · Diagenesis · Gas release · Bubbling · Bed consolidation · Oil sands

1 Introduction

The oil sands of Alberta, Canada, contain approximately 170 billion barrels of proven oil reserves. Presently, six surface mining projects are operating in the Athabasca Oil Sands Region, and other projects are at various stages of the regulatory application process. Similar to mining operations in other resource industries, oil sands mines include pit lakes in their closure and reclamation strategy. Mature fine tailings (MFT) will be placed in these pits before they are flooded with fresh water to create a lake. MFT is a mixture of fine clay materials that settle much more slowly than the coarser tailings [21], and therefore pose challenges to reclamation. Part I of this manuscript [30] discusses the overall processes that occur in oil sand pit lake sediments. A sediment diagenesis module has been developed to model these processes as well as related processes in the water column. The module has been developed by coding an add-on to CE-QUAL-W2, the US Army Corps of Engineers standard longitudinal-vertical hydrodynamic and water quality model [6–8]. The updated model is available on request at www.gemss.com/W2SedDiagenesis/W2SedDiagenesis.htm.

Physical, chemical, and biogeochemical reactions within the tailings bed in pit lakes may result in the release of aqueous and gaseous compounds into the water column, leading to

This is a two-part paper, along with *Sediment Diagenesis Module for CE-QUAL-W2. Part 1: Conceptual Formulation*

✉ Jerry A. Vandenberg
jvandenberg@golder.com

Shwet Prakash
shwet.prakash@erm.com

Edward M. Buchak
edward.buchak@erm.com

[1] ERM Inc., 75 Valley Stream Parkway, Suite 200, Malvern, PA 19355-1406, USA

[2] Golder Associates Ltd., 220 - 1755 Springfield Road, Kelowna, BC V1Y 5V5, Canada

Published online: 12 April 2015

changes in water quality. The module described herein simulates the anaerobic decay of these compounds and production of gases such as methane, carbon dioxide, and hydrogen sulfide. This paper provides details of the diagenetic process, resulting in the release of aqueous and gaseous compounds into the water column and the fate of released gases within the water column.

2 Tailings Gas Production

Prior to the early 1990s, methanogenesis had not been observed in oil sand tailing facilities. Although methanogens and sulfate-reducing bacteria had been observed in tailings samples, laboratory analyses suggested that methanogens were not likely to be active at ambient conditions in these facilities [11, 26]. In subsequent years, methanogenesis was observed in the Mildred Lake Settling Basin (MLSB) at the Syncrude Canada Ltd. oil sands operation. The reason for the time lag in the onset of methanogenesis is not known, but it may have been due to the microbially mediated depletion of sulfate, which allowed carbon to overtake sulfur as the dominant electron acceptor, or it may have been due to toxicity associated with fresh tailings that contained naphtha compounds.

Since the onset of methanogenesis, the MLSB has produced significant amounts of gases, including methane. It has been estimated that 2 to 5 % (*v*/*v*) of Mildred Lake was comprised of trapped and dissolved gases, and that gases were 20 to 60 % methane which escaped MLSB at the rate of approximately 12 g CH_4/m^2/day [14]. Holowenko et al. [15] also experimented with sulfate addition, and found that methanogens were outcompeted by sulfate-reducing bacteria, and suggested that an anticipated shift to gypsum-amended tailings might result in higher concentrations of sulfate in the tailings and a concomitant decrease in methanogenesis. Sulfate inhibition of methane production was confirmed by subsequent work, in which methanogenesis was found to occur when sulfate was consumed to levels below 20 mg/L [10].

Studies have been conducted to determine the carbon source in methane-producing tailings, and these studies have ruled out several compounds including naphthenic acids. Holowenko et al. [16] examined methanogenesis rates in the presence of various concentrations of naphthenic acids and concluded that naphthenic acids were not likely the primary carbon source of methane in tailings ponds. Furthermore, naphthenic acids did not inhibit methanogenesis due to toxicity at concentrations likely to be found in tailings ponds. Holowenko [14] amended tailings with bitumen and also observed no significant increase in methanogenesis during 516 days of incubation, indicating that bitumen was not the primary source of carbon in methanogenesis. Haveroen et al. [13] found that polyacrylamide, a chemical flocculant added to thicken tailings, may contribute to methanogenesis by providing a source of nitrogen, but that carbon was not utilized.

The main carbon source in methanogenesis is likely the solvents used in oil sand operations. Studies have documented the microbial conversion of the major naphtha components short chain n-alkanes [23] and benzene, toluene, ethylbenzene, and xylene (BTEX) compounds [22] to methane. Degradation was found to occur more rapidly in n-alkanes in the sequence $C_{10} > C_8 > C_7 > C_6$ and in BTEX compounds in the sequence toluene > xylene > ethylbenzene > benzene. Other naphtha compounds were found to be more recalcitrant within the 46-week incubation period but some were degraded with extended incubation, including long-chain alkanes [25] and iso-alkanes (J. Foght, personal communication).

Subsequent work by Siddique et al. [24] led to first- and second-order models to predict methane production in the MLSB. This model is likely not applicable to pit lakes, because it relies on a fresh input of labile BTEX or alkanes, which will not be deposited in pit lakes after mining operations cease. However, in modeling methanogenesis in pit lakes, the "conversion efficiency (η)" coefficient [24] may be applicable. This coefficient, which would be determined empirically, relates the maximum amount of carbon that is metabolized as a fraction of the total stoichiometric amount available. A value of 0.8 has been determined in microcosm experiments with fresh MFT [22, 23]; a lower value would be expected in a pit lake because the residual hydrocarbons are more resistant to biodegradation and because conditions may be sub-optimal for biodegradation. Although this coefficient is not explicitly included in the module, equivalent results could be obtained by scaling down the diagenesis rate values (see Section 2.3).

While the studies summarized above provide information on the nature of methanogenesis in mature tailings, it is not clear that tailings in pit lakes will continue to produce methane at rates currently observed in the MLSB. The literature summarized above indicates that the most applicable formulations for gas production appear to be the generic formulae provided by DiToro [9]; these formulae were adopted as the basis for the sediment module.

2.1 Overview of Diagenesis Module

The conceptualization discussed in DiToro [9] suggests that the sediment bed undergoes three basic processes. The first is diagenesis (or decay) of organic matter that consists of particulate organic carbon (POC), particulate organic nitrogen (PON), and sulfate. Both PON and POC are further subdivided into labile, refractory, and inert reaction classes based on diagenesis rates. The labile class represents rapidly decaying organic matter, the refractory class represents slowly decaying organic matter and the inert class represents any fraction of PON or POC that does not participate in the

diagenetic process. Inclusion of the inert class is required for the mass balance of the system. The second basic process is the flux of substances produced by diagenetic processes to the upper, aerobic layer and to the water column. The third and final basic process in the aerobic layer is oxidation that consumes dissolved oxygen from the water column, exerting sediment oxygen demand (SOD) on the overlying water.

There are several additional processes that can take place within the sediment bed of pit lakes, as discussed individually in the following sections. Since these processes were not part of the standard DiToro [9] diagenesis formulations, they have been added to the module. A schematic of all chemical reactions included in the diagenesis module is provided in Fig. 1. The schematic shows a two-layer formulation that separately accounts for POC, PON, and sulfide under both aerobic and anaerobic conditions within the sediment bed. It illustrates transport and transformation pathways of these compounds within the sediment and upwards into the water column.

The two-layer formulation (Fig. 2) employs an aerobic top layer (upper layer) and an anaerobic bottom layer (lower layer). The upper layer has a varying depth determined by the depth of oxygen penetration from the overlying water column. Under conditions of no oxygen in the overlying water column, the upper layer may be anaerobic. The presence of oxygen in the upper layer controls all oxidation processes in this layer, as described in the following sections. Thus, when oxygen is absent in this layer, anaerobic process may occur there. Even at its maximum thickness, the upper layer is a small fraction of the total sediment bed in terms of volume.

The lower layer is always anaerobic and is the predominant source of diagenetic fluxes. The thickness of this lower layer is kept constant in the DiToro formulations [9]. However, the diagenesis module includes a consolidating sediment bed and changes were made to the DiToro formulation to accommodate spatially and time-varying bed thickness. The sediment bed is thus represented using two fully mixed (homogeneous) sediment layers varying in thickness with time and space.

The assumption of homogeneous sediment layer was made to simplify the complex diagenetic processes. Vertical heterogeneity is possible in deep sediment beds where diagenesis may be different in deeper parts of the bed compared to shallower parts of the bed. This simplification can be addressed by the addition of "lower" layers. At the time of this model development, insufficient information is available to parameterize, implement, and validate heterogeneous layers. Gas releases as part of the overall diagenetic process are known and are only sufficient to validate a homogenous sediment bed.

The equations developed for the module rely on the principle of mass balance. The mass balance principle requires that the mass of any constituents within a control volume must be the result of sources of mass to the volume, less the losses within the volume, and the export from the volume. Note that the equations shown in this report assume a limitless supply of water and protons, so these are omitted from the chemical reactions and mass balances shown below.

The mass balance equations for the two-layer model for a constituent C are shown in Eq. 1 (for upper layer) and Eq. 2 (for lower layer).

$$H_1\frac{dC_1}{dt} = J_1 + K_{L12}(C_2 - C_1) + K_{L01}(C_0 - C_1) - K_{r1}C_1 \quad (1)$$

$$H_2\frac{dC_2}{dt} = J_2 + K_{L12}(C_1 - C_2) - K_{r2}C_2 \quad (2)$$

where H is the layer thickness, J is the production (source) flux, and K_r is the decay/reaction loss for constituent C. Subscripts 1 and 2 denote the values for the upper and lower layers, respectively. K_{L12} is the mass transfer (diffusion) coefficient between the upper and lower layers. C_0 is the concentration in the overlying water column and K_{L01} is the mass transfer coefficient between the upper layer and the water column.

The thickness of the upper layer is much smaller than in the lower layer. Due to the difference in thickness, the mass of POC and PON within the upper layer is not included in the overall mass balance, although the mass of reaction products in this layer is accounted for.

Diagenetic processes are, among other factors, temperature- and pressure-dependent. Temperature dependence has been implemented for all various reactions discussed in the following section using the temperature correction discussed in Section 2.5. However, the pressure dependence has not been explicitly included. The reaction rates for all diagenetic processes are defined as user input and can be specified as spatially and temporally varying rates. It is assumed that the model will be set up with calibrated rates representing the pressure dependence. In future updates, pressure dependence can be included as part of heterogeneous layers for the sediment bed.

2.2 Particulate Organic Nitrogen

PON in the sediment bed decreases in concentration as a consequence of mineralization to ammonia (Eq. 3). Ammonia (NH_3) may be oxidized to nitrate (NO_3^-), but only in the upper layers where oxygen is available for the reaction. Ammonia also undergoes ionization (NH_3 to NH_4^+), depending on a user-specified pH of the pore water. Finally, ammonia may undergo dissolution ($NH_{3(g)}$ to $NH_{3(aq)}$) according to Henry's Law.

$$\mathrm{PON} \xrightarrow{k_{PON}} \mathrm{NH_4^+} \quad (3)$$

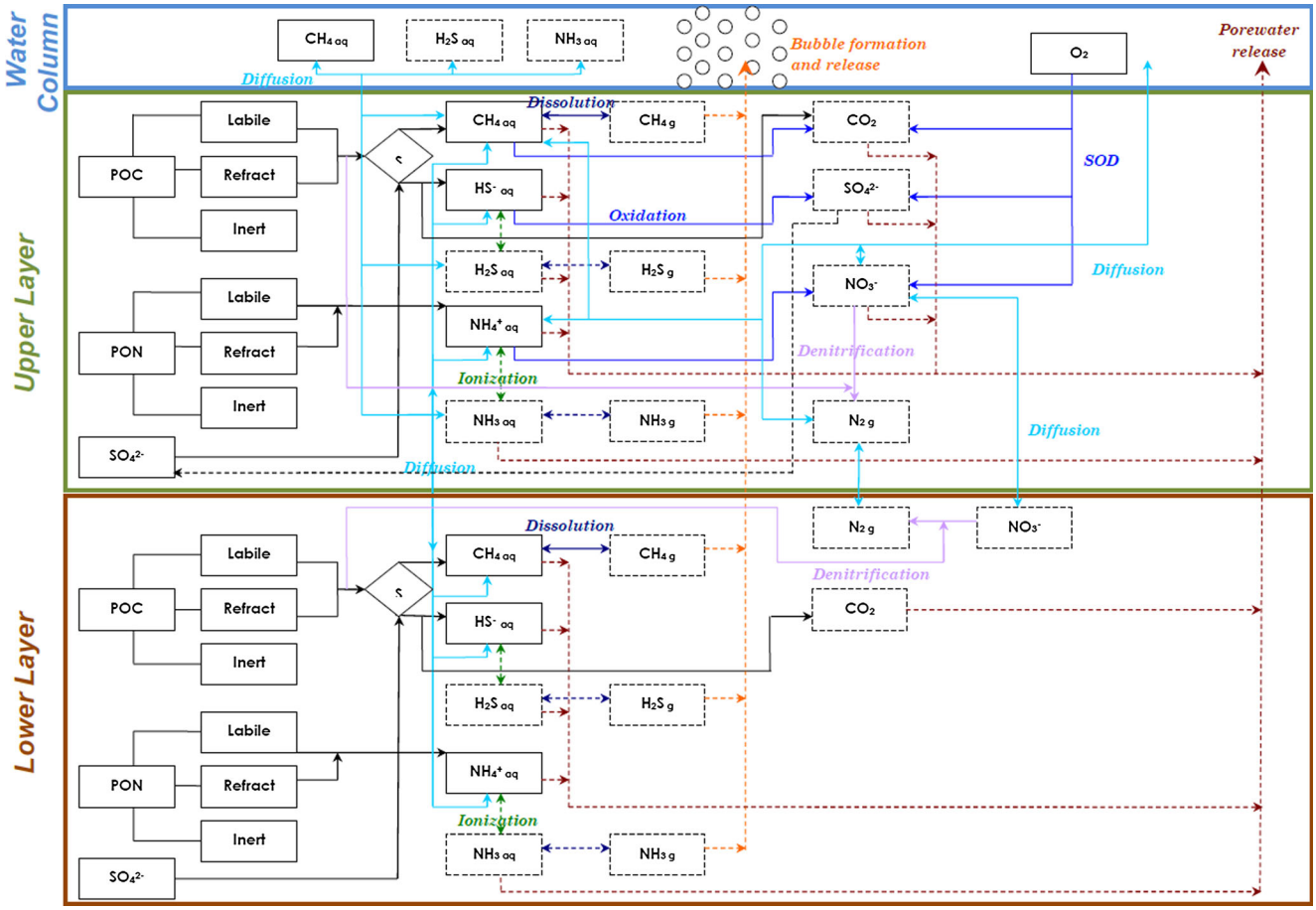

Fig. 1 Diagenesis framework showing the two-layer module based on DiToro (2001). Figure illustrates the transport and transformation pathways of compounds in sediment and upwards to water column. *POC* particulate organic carbon, *PON* particulate organic nitrogen, *SOD* sediment oxygen demand, *aq* aqueous, *g* gaseous; *solid lines* indicate processes from DiToro (2001); *dashed lines* indicate additional processes added to module

The mass balance equation for PON in the lower layer is given by Eq. 4.

$$H_2\frac{d\mathrm{PON}_2}{dt} = -k_{\mathrm{PON2}}H_2\mathrm{PON}_2 \tag{4}$$

where k_{PON} is the diagenesis rate.

Ammonia may be transferred to the overlying water via diffusion from porewater, depending on the concentration of ammonia in the overlying water. Ammonia is similarly transferred between the upper and lower layers, depending on the concentration gradient between the two. The mass balance equations for ammonia in the upper and lower layers are given by Eqs. 5 and 6.

$$H_1\frac{d\mathrm{NH}_{4,1}}{dt} = +k_{\mathrm{PON1}}H_1\mathrm{PON}_1 - K_{\mathrm{L01}}\left(\mathrm{NH}_{4,1} - \mathrm{NH}_{4,0}\right) + K_{\mathrm{L12}}\left(\mathrm{NH}_{4,2} - \mathrm{NH}_{4,1}\right) - k_{\mathrm{NH4,1}}H_1\mathrm{NH}_{4,1} \tag{5}$$

$$H_2\frac{d\mathrm{NH}_{4,2}}{dt} = +k_{\mathrm{PON2}}H_2\mathrm{PON}_2 - K_{\mathrm{L12}}\left(\mathrm{NH}_{4,2} - \mathrm{NH}_{4,1}\right) \tag{6}$$

where K_{L01} and K_{L12} are the mass transfer coefficients for ammonia at the sediment–water and upper-lower interfaces, $k_{\mathrm{NH4,1}}$ is the nitrification rate for the upper layer, and $\mathrm{NH}_{4,0}$ is the concentration of ammonia in the overlying water column.

The nitrification reaction rate follows Monod kinetics with respect to the ammonia and oxygen concentrations—the rate of nitrification decreases as the ammonia concentration increases. Similarly, the nitrification reaction decreases with decreasing oxygen concentrations. This phenomenon can be represented by combining the two effects to modify the nitrification rate as shown in Eq. 7.

$$k_{\mathrm{NH}_{4,1}} = k_{N\mathrm{H}_{4,1\text{-optimum}}} \times \frac{K_{\mathrm{M,NH}_4}}{K_{\mathrm{M,NH}_4} + \mathrm{NH}_{4,1}} \times \frac{\mathrm{O}_{2,1}}{K_{\mathrm{M,O}_2} + \mathrm{O}_{2,1}} \tag{7}$$

where $K_{\mathrm{NH4,1\text{-optimum}}}$ is the nitrification rate at optimum ammonia and oxygen concentrations, $K_{\mathrm{M,NH4}}$ is the half-saturation constant for ammonia, and $K_{\mathrm{M,O2}}$ is the half-saturation constant for oxygen.

Nitrate (NO_3^-) produced from the diagenetic process may be denitrified to nitrogen gas ($N_{2(g)}$) in either layer. Denitrification is an anaerobic process that may occur in the upper layer when

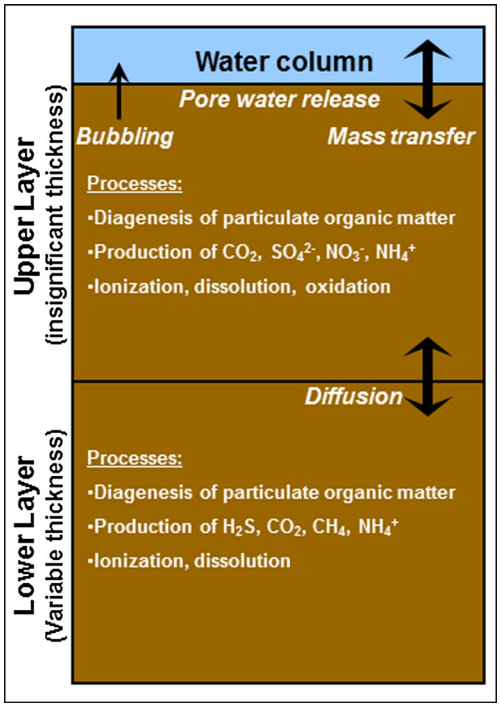

Fig. 2 Conceptual diagram of two-layer sediment diagenesis model implemented in the module

DO concentrations are low enough to change the upper layer into an anaerobic layer. Nitrogen gas may pass between layers and diffuse to the overlying water, depending on concentration gradients between layers. Equations 8 and 9 show the mass balances for nitrate in the upper and lower layers, respectively.

$$H_1\frac{dNO_{3,1}}{dt} = +k_{NH4,1}H_1NH_{4,1} - K_{L01}\left(NO_{3,1} - NO_{3,0}\right) + K_{L12}\left(NO_{3,2} - NO_{3,1}\right) - k_{NO3,1}H_1NO_{3,1} \quad (8)$$

$$H_2\frac{dNO_{3,2}}{dt} = -k_{NO_{3,2}}H_2NO_{3,2} - K_{L12}\left(NO_{3,2} - NO_{3,1}\right) \quad (9)$$

where $k_{NO3,1}$ and $k_{NO3,2}$ are the denitrification rates for upper and lower layers. Kinematic rates and constants associated with these processes are read from the input file. The diagenesis module allows spatially varying rates to provide flexibility in specifying sediment bed properties.

2.3 Particulate Organic Carbon

Methane (CH_4) and carbon dioxide (CO_2) are produced by the anaerobic decay of POC involving a consortium of microbes. In the upper zone, methane can be oxidized by methanotrophic microbes to produce CO_2 and H_2O. As mentioned previously, sulfate inhibition of methanogenesis has been found to occur when the sulfate concentration was above 20 mg/L [10]. Based on these observations, a user-specified, sulfate inhibition concentration was added to the model, with a default value of 20 mg/L of sulfate. Below this value, methanogenesis occurs (Eq. 10). Above this value, consumption of POC occurs while reacting with sulfate to form sulfide. The conversion efficiency (η) coefficient described by [24] can be applied to Eq. 11 by modifying the diagenesis rate. Additionally, the fraction of labile and refractory can be controlled to implement this factor more closely.

$$POC \rightarrow CO_2 + CH_4 \quad (10)$$

The mass balance equation for POC in the lower layer can be given by Eq. 11. Note that POC cannot be added to the sediments after the start of the simulation.

$$H_2\frac{dPOC_2}{dt} = -k_{POC2}H_2POC_2 \quad (11)$$

where k_{POC} is the diagenesis rate.

Oxidation of methane may occur in the upper layer, which then exerts an oxygen demand on the overlying water column. Microbial oxidation of dissolved methane consumes oxygen and produces CO_2 (Eq. 12). Transport of methane within interstitial water is through diffusion, as methane is only slightly soluble in water. Methane may also be transported along with clay and bitumen to which it strongly sorbs, but this transport mechanism is not presently included in the model. When methane's solubility is exceeded in interstitial water, it forms a gas that escapes as bubbles. The relationship between the dissolved and gaseous forms is defined by Henry's Law. A similar relationship is written for the produced carbon dioxide, although dynamic pH interactions are not presently included. Equations 13 and 14 show the mass balance equations for methane in both layers. S_{CH4} is the methane production flux for each layer and K_{CH4} with subscripts 1 and 2 are the methane oxidation rates for the upper and lower layers.

$$CH_4 + O_2 \rightarrow CO_2 + H_2O \quad (12)$$

$$-D_{CH_{4,1}}\frac{d^2CH_{4,1}}{dz^2} = -K_{CH_{4,1}}CH_{4,1} + S_{CH_{4,1}} \quad (13)$$

$$-D_{CH_{4,2}}\frac{d^2CH_{4,2}}{dz^2} = S_{CH_{4,2}} \quad (14)$$

where $D_{CH4,1}$ is the diffusivity of methane in the upper zone of the sediment bed, z is the depth within the bed, and S is the rate of carbon diagenesis in oxygen equivalents.

Mass balance equations for both upper and lower layers are formed similar to those for PON. If sulfate formation is occurring, then the sediment bed sulfate concentration increases with sulfide consumption. The module allows spatially varying rates to provide flexibility in specifying sediment bed properties.

2.4 Sulfate

Consumption of sulfate to produce sulfide is shown in Eq. 15.

$$\mathrm{POC} + \mathrm{SO_4^{2-}} \rightarrow \mathrm{CO_2} + \mathrm{HS^-} \tag{15}$$

In the module, any sulfide formed may undergo reversible ionization (HS^- to H_2S), depending on the user-specified pH of the pore water. Hydrogen sulfide can exist in both dissolved and gaseous phases. The upper layer experiences oxidation of sulfide to give sulfate (Eq. 16). The sulfate produced from sulfide consumption contributes to the total sulfate content.

$$\mathrm{H_2S} + \mathrm{O_2} \rightarrow \mathrm{H_2SO_4} \tag{16}$$

The mass balance equation for sulfate in the upper and lower layers can be represented by Eqs. 17 and 18 and for sulfide in the upper and lower layers by Eqs. 19 and 20.

$$\mathrm{H_1}\frac{d\mathrm{SO_{4,1}}}{dt} = +k_{\mathrm{HS1}}\mathrm{H_1HS_1} - K_{\mathrm{L01}}\left(\mathrm{SO_{4,1}} - \mathrm{SO_{4,0}}\right) + K_{\mathrm{L12}}\left(\mathrm{SO_{4,2}} - \mathrm{SO_{4,1}}\right) - k_{\mathrm{SO4,1}}\mathrm{H_1SO_{4,1}} \tag{17}$$

$$\mathrm{H_2}\frac{d\mathrm{SO_{4,2}}}{dt} = -k_{\mathrm{SO4,2}}\mathrm{H_2SO_{4,2}} - K_{\mathrm{L12}}\left(\mathrm{SO_{4,2}} - \mathrm{SO_{4,1}}\right) \tag{18}$$

$$\mathrm{H_1}\frac{d\mathrm{HS_1}}{dt} = +k_{\mathrm{SO4,1}}\mathrm{H_1SO_{4,1}} - K_{\mathrm{L01}}(\mathrm{HS_1} - \mathrm{HS_0}) + K_{\mathrm{L12}}(\mathrm{HS_2} - \mathrm{HS_1}) - k_{\mathrm{HS1}}\mathrm{H_1HS_1} \tag{19}$$

$$\mathrm{H_2}\frac{d\mathrm{HS_2}}{dt} = +k_{\mathrm{SO4,2}}\mathrm{H_1SO_{4,2}} - K_{\mathrm{L12}}(\mathrm{HS_2} - \mathrm{HS_1}) \tag{20}$$

2.5 Temperature Correction

The rates of reactions applied in the diagenesis formulations are generally temperature dependent, and this dependence can be defined by Eq. 21.

$$k = k_r\theta^{(T-20)} \tag{21}$$

where k_r is the reaction rate, θ is the temperature coefficient, and T is the temperature.

Reaction rates in the diagenesis formulations applied in the module make use of this temperature-dependent relationship. Temperature is routinely computed by CE-QUAL-W2.

2.6 Ionization

Diagenesis products such as sulfide and ammonia can undergo ionization based on their ionization potential and water pH. Currently, the module keeps pore water pH constant with time; future upgrades may include a calculation of a time-varying pH in pore water. Ionization of ammonia in pore water occurs according to Eq. 22.

$$\mathrm{NH_4^+} \leftrightarrow \mathrm{NH_3} + \mathrm{H^+} \tag{22}$$

Under equilibrium conditions, the concentration of individual reactants and products can be written according to Eq. 23

$$K \leftrightarrow \frac{[\mathrm{NH_3}][\mathrm{H^+}]}{[\mathrm{NH_4^+}]} \tag{23}$$

where $[H^+]$ can be defined by pH and calculated by Eq. 24

$$\mathrm{pH} = -\log_{10}[\mathrm{H^+}] \tag{24}$$

The equilibrium constant (K) is input as pK which is defined by Eq. 25.

$$pK = -\log_{10}[K] \tag{25}$$

3 Bubbling to Surface

The physics of bubble formation and escape from sediments has not been studied in detail in oil sand pit lakes. However, multi-phase systems have been studied in the context of contaminated sites, methane hydrate recovery, and greenhouse gas accounting. The results of these studies, which were reviewed to inform the development of a bubble formation framework for the module, are summarized briefly in the following section.

3.1 Review of Bubble Dynamics Studies

The formation of gas bubbles in sediments and release to the overlying water column is described by van Kesteren and van Kessel [28] in their work relating to harbor sludge. Gases were produced by methanogenesis, which increased the concentration of those gases in interstitial waters within the sediments. In fine sediments, advective and diffusive transport of gases from the interstitial waters was very slow. Produced gases led to higher dissolved gas concentrations up to the point of saturation, at which point, bubbles formed. Bubbles continued to grow until the upward force on the sediment exceeded the fracture energy, at which point, the bubbles escaped to the overlying water column.

While van Kesteren and van Kessel [28] indicated that bubbles form until they create cracks in the matrix, at which time, the bubbles escape the sediments, subsequent work indicated that bubbles will escape when the bulk density of the sediments is less than the bulk density of water [29]. This latter explanation may have more relevance for MFT, which

has low shear strength. Tailings have been described as MFT if the shear strength is less than 10 kPa, although a more detailed analysis indicated that aged MFT would have a shear strength of less than 50 Pa near the surface and approximately 5000 Pa near the bottom [27].

Methane bubble formation in muddy marine sediments has been studied using x-ray computed tomographic images [3]. Bubbles were found to form oblate spheroids, then fracture the sediment when internal bubble pressure rose above a critical pressure. In response to bubble growth, muddy sediment was found to act as a solid and fracture, whereas sandy sediments responded more like a fluid. Bubbles formed according to mechanics predicted by earlier work as per the linear elastic fracture mechanics (LEFM) model [12, 18]. The LEFM model was solved as a transient model using the finite-element method [1] to overcome the quasi-steady state assumption from earlier work. The LEFM model predicts bubble size and growth rate as a function of methane production rate and physical characteristics of the sediment. Growth rates computed by this model were comparable to field observations from other studies [19, 20]. While the LEFM model is applicable to the micro-scale of bubble formation, and the current modeling effort is applicable to the macro-scale, the LEFM model may be of use in validating certain aspects of the bubble dynamics predicted by the module, such as overall growth rate and volume.

Bubble-facilitated transport of solid- and gas-phase contaminants has been examined in the laboratory by measuring the amount of phenanthrene transferred by bubbles from the sediment to the overlying water column in column experiments [32]. Re-suspension of total suspended solids (TSS) due to ebullition was observed but was not quantitatively measured. Yuan et al. [33] continued this work with additional column experiments and the development of a mathematical transport model. This model was used to predict the transfer of contaminants from sediments to the water column and atmosphere. This model was developed primarily to assess sediment capping as a mitigation measure for contaminated sediments. Based on the results of these laboratory tests, Yuan et al. [32] concluded that bubble-mediated transport was not likely to contribute significant amounts of contaminants compared to other modes of transport such as bioturbation. However, depending on the ebullition rates predicted for pit lakes, which may exceed those observed in natural systems, bubble-mediated transport of contaminants may be a dominant process, and was included mechanistically in the module. Phenomenon of gas release from specific locations is reproduced by having a longitudinally discretized model grid (2-D). However, lateral variations can only be reproduced if the model discretization is three-dimensional. A possible future upgrade for the sediment diagenesis module is to implement it into a 3-D model.

3.2 Model Formulation of Bubble Formation and Release

Continuous production of dissolved gases (H_2S, CH_4, CO_2, and NH_3) through diagenesis may result in oversaturation, at which point bubbles may form. The relationship between the dissolved and gaseous phase is described by Henry's Law. The solubility of each gas determines the amount of gas formed in the interstitial pores. In situ rates of bubble formation have not been measured in MFT, and thus the module relies on generic bubble formation and growth relationships. The growth model adopted for the module is based on the work of Boudreau et al. [4, 5]. This model was chosen because it considers a distributed source of gas formation which is not normally included in other bubble growth models. This approach is important as the sediment bed continually produces gas through diagenesis. The authors note that the validity of the model is restricted by its assumptions but that the results are correct within an order of magnitude even if some of the assumptions are violated. A complete bubble creation and release model would include nucleation, kinetics of gas adsorption, transport of the gas, and mechanical response of the sediments. However, nucleation kinetic limitations are overcome by assuming that there are abundant nucleation sites and that the bubbles form without hindrance. Similarly, the rate of growth of bubbles in sediments is sufficiently slow that adsorption kinetics can be ignored. This assumption leaves only transport and mechanical controls to be considered.

In order to describe the sediment bubble system, the bubble-in-a-continuum model proposed by Wheeler [31] was adopted for inclusion in the module, wherein a bubble is a discrete gaseous entity that is embedded in a sediment–pore water continuum, as in a classical diagenetic model [2]. The bubble is assumed to be spherical. In cases where bubbles take other shapes (e.g., disc shaped as discussed in [12]), the present model is simply an approximation using a spherical bubble of equivalent volume. Detailed formulation of the bubble growth model is provided by Boudreau et al. [4, 5]. The rate of change of bubble radius obtained from the Boudreau model is shown in Eq. 26:

$$\frac{dR}{dt} = \frac{\phi D}{RC_g}\left\{\frac{SR_1^2}{6D} + (C_1 - C_o)\right\} \tag{26}$$

where φ is sediment bed porosity, D is diffusivity of gas in the sediment bed, R is bubble radius, C_g is concentration of gas in the bubble, S is gas production rate, R_1 is a calibration parameter, C_1 is concentration of each dissolved gas at a distance farther away from the site of nucleation (background concentration), and C_0 is concentration of each dissolved gas at the bubble surface (assumed to be in the pore water next to the bubbles).

Using Eq. 26, a relationship can be obtained for use in the module where the bubble radius is calculated at each time step. The relationship is shown in Eq. 27:

$$R_b^{n+1} = R_b^n + \frac{\phi D}{R_b^n C_g}\left\{\frac{SR_1^2}{6D} + (C_1 - C_o)\right\}\Delta t \tag{27}$$

where R_b^{n+1} is bubble radius at time step $n+1$, R_b^n is bubble radius at time step n, and Δt is time step.

The concentration of gas (C_g) and the dissolved concentration at the bubble surface are always in equilibrium and are related by Henry's Law as shown in Eq. 28:

$$C_g = C_0 K_i \tag{28}$$

where K_i is the equilibrium constant for gas i, shown in Eq. 29:

$$K_i = H_i/(RT) \tag{29}$$

where H_i is Henry's constant for gas i, R is the universal gas constant, and T is temperature in Kelvin.

Bubble growth in an elastic medium that is susceptible to fracture occurs in two different ways, as described by [12]. If the internal gas pressure is lower than the critical value given by the strength of the material, then the bubble will expand as it receives gas by diffusion from the surrounding pore water; i.e., the sediment will compress elastically as pressure builds in the bubble (the elastic phase). When the internal pressure exceeds the strength of the sediment, the sediment will fracture and the gas bubbles will be released. The critical pressure at which bubbles result in sediment fracture (crack formation) is given by Eq. 30 based on Gardiner et al. [12]:

$$P_{\text{crit}} = \frac{\pi^{4/5} K_{1c}^{6/5}}{24^{1/5}(EV)^{1/5}} + P_o \tag{30}$$

where K_{1c} is the critical stress intensity factor and E is Young's modulus, V is bubble volume, and P_0 is the background pressure. The background pressure is the water column pressure overlying the sediment bed. Cracks would form sooner in shallow lakes compared to deep lakes as the water column above the sediment bed will exert pressure that will contribute toward the bed's compactness.

Existing models do not consider the closing of these cracks under pressure from the overlying water column. To address this shortcoming, the formed cracks in the sediment bed are closed at a fraction of the critical pressure. The fraction is user-defined and can be used as a calibration parameter. Once the cracks close, additional bubbles are not released and bubble pressure starts to increase again until the cracks reoccur.

3.3 Bubble-Induced Turbulence

While many studies have been carried out to understand bubble-induced turbulence, our knowledge is still insufficient for developing accurate models on the effects of bubbles on turbulence properties in bubbly flows [17]. The addition of turbulence resulting from gases bubbling from the sediment bed is based on the two-phase bubbly flow algorithms used in modeling industrial processes of gas exchange in chemical reactors, aeration tanks, and heat exchangers. To model such processes, a multi-phase calculation would need to be adopted in which two separate fluid phases (water and gas) are considered. Inclusion of such an approach was beyond the scope of current effort as it would require re-development of the fundamental structure of CE-QUAL-W2. However, a simplified correction that accounts for bubble-induced turbulence based on the turbulence viscosity [17] has been adopted for the module. The momentum equation used in CE-QUAL-W2 is shown in Eq. 31:

$$\frac{DU}{Dt} = -\frac{\nabla P}{\rho} + \nabla \nu_t(\nabla U) + g \tag{31}$$

where P is the pressure, ρ is the density of water, U is the velocity vector (u, v, and w in the direction of x, y, and z axis) and g is the acceleration due to gravity. The turbulent viscosity, ν_t, can be modified to include the bubble-induced turbulence. The net turbulent viscosity in a bubbly flow can be calculated using Eq. 32:

$$\nu_{\text{net}} = \nu_t + \nu_b \tag{32}$$

where ν_b is the bubble-induced turbulence that can be given by Eq. 33.

$$\nu_b \propto d_b \times V_R \tag{33}$$

where d_b is the average bubble diameter and V_R is the average rise velocity.

Table 1 Formulae used to determine Reynolds number [34]

Range	Reynolds number formula
$N_D \leq 73$	$R = \frac{N_D}{24} - 1.7569 \times 10^{-4} N_D^2 + 6.9252 \times 10^{-7} N_D^3 - 2.3027 \times 10^{-10} N_D^4$
$73 < N_D \leq 580$	$\log R = -1.7095 + 1.33438W - 0.11591W^2$
$580 < N_D \leq 1.55 \times 10^7$	$\log R = -1.81391 + 1.34671W - 0.12427W^2 + 0.006344W^3$
$N_D = 4\rho\Delta\rho g d_e^3/3\mu^2$ and $W = \log N_D$	

A scaling factor (φ) is added to obtain a relationship to calculate bubble-induced turbulence as shown in Eq. 34.

$$\nu_b = \phi \times d_b \times V_R \tag{34}$$

3.4 Bubble Rise and Release

Once the bubbles are released into the water column, they rise due to the buoyancy forces acting on them. Due to the wide range of possible gas bubble sizes rising from the sediment bed, the more general formulations of Zheng and Yapa [34] were adopted for use in the module. Although spherical bubbles are modeled in the module, the rise velocity computations [34] are also applicable to non-spherical bubbles. In the case of non-spherical bubbles, an equivalent spherical diameter (d_e) for the bubble is used. The following equations show the calculation of rise velocity (V_r) and have been taken directly from Zheng and Yapa [34].

For bubbles of small size range ($d_e \leq 1$ mm)

$$V_r = \frac{R\mu}{\rho d_e} \tag{35}$$

where μ is the dynamic viscosity of gas, ρ is the density of water, and R is the Reynolds number (Table 1).

For bubbles of intermediate size range (1 mm$<d_e\leq$ 15 mm)

$$V_r = \frac{\mu}{\rho d_e} M^{-0.149(J-0.857)} \tag{36}$$

$$H = \frac{4}{3} E_o M^{-0.149} \left(\frac{\mu}{\mu_w}\right)^{-0.14} \tag{37}$$

$$M = g\mu^4 \Delta\rho / \rho^2 \sigma^3 \tag{38}$$

$$E_o = g\Delta\rho d_e^2 / \sigma \tag{39}$$

$$J = 0.94 H^{0.757} \text{ when } 2 < H \leq 59.3 \tag{40}$$

$$J = 3.42 H^{0.441} \text{ when } H > 59.3 \tag{41}$$

H, M, E_o, and J are intermediate velocity calculation variables, and σ is the interfacial tension.

For bubbles of large size range ($d_e>18$ mm)

$$V_r = 0.711\sqrt{g d_e \Delta\rho / \rho} \tag{42}$$

Rise velocity for bubbles between the size of 15 and 18 mm is calculated by linearly interpolating between the rise velocity at 15 mm using Eq. 36 and 18 mm using Eq. 42. Reynolds number (R) for bubbles can be calculated using formulations given in Table 1.

The bubbles exchange gases with the water during their transit through the water column. Once the bubbles rise to the water surface, a burst factor is applied that represents the bubbles bursting and releasing gases to the atmosphere. The same factor controls the duration of the bubbles in the water column.

The exchange of gases between the bubbles and the water column is calculated using a gas transfer coefficient. The equilibrium dissolved concentration for the gases are calculated for the bubbles based on Henry's Law, as per Eq. 43:

$$C_{\mathrm{Eq}b-d-i} = C_{\mathrm{bubble}-i} / K_i \tag{43}$$

where $C_{\mathrm{Eq}b\text{-}d\text{-}i}$ is the equilibrium concentration in dissolved phase for gas i in the bubble, $C_{\mathrm{bubble}\text{-}i}$ is the concentration in gaseous phase for gas i in the bubble, and K_i is the equilibrium constant for gas i.

Flux of gas from bubble to water for gas i is obtained through Eq. 44:

$$J_{g-w-i} = K_{g-w-i}\left(C_{\mathrm{Eq}b-d-i} - C_{d-i}\right) \tag{44}$$

where $J_{g\text{-}w\text{-}i}$ is the flux, $K_{g\text{-}w\text{-}i}$ is the gas transfer coefficient for gas i, and $C_{d\text{-}i}$ is the dissolved concentration of gas i.

4 Conclusions

The diagenesis module has been developed to mechanistically model digenetic processes in pit lakes. The module includes several physico-chemical processes that have been observed in tailings ponds and other similar systems, such as degradation of organic compounds, gas generation, bubble formation, ebullition, and gas exchange with bubbles in the water column. The formulations and rates are based on field observations, literature values from similar systems, and calibration parameters. Although these model formulations and processes need to be validated at laboratory or pilot scale, the model framework provides a valuable tool in determining the fate of such pit lakes.

Acknowledgments This model development was funded by the Cumulative Environmental Management Association (CEMA), which is a multi-stakeholder group that is tasked with studying cumulative effects in Alberta's oil sand region and making recommendations for regulatory agencies. The authors wish to thank CEMA and its members for funding this study. In addition, the authors wish to thank CEMA's End Pit Lake Task Group and the three external reviewers for providing insightful reviews of this manuscript.

References

1. Algar, C. K., & Boudreau, B. P. (2009). Transient growth of an isolated bubble in muddy, fine-grained sediments. *Geochimica et Cosmochimica Acta, 73*(9), 2581–2591.
2. Boudreau, B. P. (1997). *Diagenetic models and their implementation*. Berlin: Springer Verlag. 414 p.
3. Boudreau, B. P., Algar, C., Johnson, B. D., Croudace, I., Reed, A., Furukawa, Y., Dorgan, K. M., Jumars, P. A., Grader, A. S., & Gardiner, B. S. (2005). Bubble growth and rise in soft sediments. *Geology, 33*(6), 517–520.
4. Boudreau, B. P., Gardiner, B. S., & Johnson, B. D. (2001). Rate of growth of isolated bubbles in sediments with a diagenetic source of methane. *Limnology and Oceanography, 46*(3), 616–622.
5. Boudreau, B. P., Gardiner, B. S., & Johnson, B. D. (2001). Errata to rate of growth of isolated bubbles in sediments with a diagenetic source of methane. *Limnology and Oceanography, 46*(6), 1578.
6. Buchak, E. M., & Edinger, J.E. (1984). *Generalized, longitudinal-vertical hydrodynamics and transport: development, programming and applications*. Prepared for U.S. Army Corps of Engineers Waterways Experiment Station, Vicksburg, Mississippi. Contract No. DACW39-84-M-1636. Prepared by J. E. Edinger Associates, Wayne, Pennsylvania 19087–3226. Document No. 84-18-R. June.
7. Cole, T. M., & Buchak, E. M. (1995). *CE-QUAL-W2: a two-dimensional, laterally averaged, hydrodynamic and water quality model, Version 2.0* (Instruction Report EL-95-1). Vicksburg: US Army Engineer Waterways Experiment Station.
8. Cole, T.M., & Wells, S.A. (2008). *CE-QUAL-W2: a two-dimensional, laterally averaged, hydrodynamic and water quality model, version 3.6*. Prepared for U.S. Army Corps of Engineers, Washington, DC 20314-1000.
9. DiToro, D. M. (2001). *Sediment flux modeling*. New York: Wiley-Interscience. 656pp.
10. Fedorak, P. M., Coy, D. L., Salloum, M. J., & Dudas, M. J. (2002). Methanogenic potential of tailings samples from oil sands extraction plants. *Canadian Journal of Microbiology, 48*, 21–33.
11. Foght, J. M., Fedorak, P. M., & Westlake, D. W. S. (1985). Microbial content and metabolic activities in Syncrude tailings pond. *AOSTRA Journal of Research, 1*, 139–146.
12. Gardiner, B. S., Boudreau, B. P., & Johnson, B. D. (2003). Growth of disk-shaped bubbles in sediments. *Geochimica et Cosmochimica Acta, 67*, 1485–1494.
13. Haveroen, M. E., MacKinnon, M. D., & Fedorak, P. M. (2005). Polyacrylamide added as a nitrogen source stimulates methanogenesis in consortia from various wastewaters. *Water Research, 39*(14), 3333–3341.
14. Holowenko, F.M. (2000). *Methanogenesis and fine tailings waste from oil sands extraction: a microcosm-based laboratory examination*. M.Sc. Thesis. University of Alberta. Edmonton, Ab. 203pp.
15. Holowenko, F. M., MacKinnon, M. D., & Fedorak, P. M. (2000). Methanogens and sulfate-reducing bacteria in oil sands fine tailings waste. *Canadian Journal of Microbiology, 46*(10), 927–937.
16. Holowenko, F. M., MacKinnon, M. D., & Fedorak, P. M. (2001). Naphthenic acids and surrogate naphthenic acids in methanogenic microcosms. *Water Research, 35*, 2595–2606.
17. Hosokawa, S., & Tomiyama, A. (2010). *Effects of bubbles on turbulent flows in vertical channels*. Tampa: 7th International Conference on Multiphase Flow. ICMF 2010.
18. Johnson, B. D., Boudreau, B. P., Gardiner, B. S., & Maass, R. (2002). Mechanical response of sediments to bubble growth. *Marine Geology, 187*, 347–363.
19. Klein, S. (2006). Sediment porewater exchange and solute release during ebullition. *Maritime Chemistry, 102*, 60–71.
20. Martens, C. S., & Klump, J. V. (1980). Biogeochemical cycling in an organic-rich coastal marine basin-I. Methane sediment-water exchange processes. *Geochimica et Cosmochimica Acta, 44*, 471–490.
21. Mikula, R.J., Kasperski, K.L., Burns, R.D., & MacKinnon, M.D. (1996). Nature and fate of oil sands fine tailings. In: *Schramm, L.L., Suspensions: Fundamentals and Applications in the Petroleum Industry. American Chemical Society.*
22. Siddique, T., Fedorak, P. M., MacKinnon, M. D., & Foght, J. M. (2007). Metabolism of BTEX and naphtha compounds to methane in oil sands tailings. *Environmental Science & Technology, 41*, 2350–2356.
23. Siddique, T., Fedorak, P. M., & Foght, J. M. (2006). Biodegradation of short-chain n-alkanes in oil sands tailing under methanogenic conditions. *Environmental Science & Technology, 40*, 5459–5464.
24. Siddique, T., Gupta, R., Fedorak, P. M., MacKinnon, M. D., & Foght, J. M. (2008). A first approximation model to predict methane generation from an oil sands tailings settling Basin. *Chemosphere, 72*, 1573–1580.
25. Siddique, T., Penner, T., Semple, K., & Foght, J. M. (2011). Anaerobic biodegradation of longer-chain n-alkanes coupled to methane production in oil sands tailings. *Environmental Science & Technology, 45*, 5892–5899.
26. Sobolewski, A. (1992). *The microbial characteristics of oil sands tailings sludge*. Calgary: Consultant's report submitted to AOSTRA.
27. Suthaker, N.N. (1995). *Geotechnics of oil sand fine tailings*. Ph.D. Thesis. University of Alberta, Edmonton, AB.
28. van Kesteren, W., & van Kessel, T. (2002). Gas bubble nucleation and growth in cohesive sediments. In J. C. Winterwerp & K. Kranenburg (Eds.), *Fine sediment dynamics in the marine environment. Proc Marine Science 5* (pp. 329–341). Amsterdam: Elsevier.
29. van Kesteren, W., & van Kessel, T. (2002). Gas production and transport in artificial sludge depots. *Waste Management, 22*, 19–28.
30. Vandenberg, J. A., Prakash, S., & Buchak, E. (2014). Sediment diagenesis module for CE-QUAL-W2. Part 1: conceptual formulation. *Environmental Modeling and Assessment*. doi:10.1007/s10666-014-9428-0.
31. Wheeler, S. J. (1988). A conceptual model for soils containing large gas bubbles. *Geotechnical, 38*, 389–397.
32. Yuan, Q. Z., Valsaraj, K. T., Reible, D. D., & Willson, C. S. (2007). A laboratory study of sediment and contaminant release during gas ebullition. *Journal of the Air and Waste Management Association, 57*, 1103–1111.
33. Yuan, Q. Z., Valsaraj, K. T., & Reible, D. D. (2009). A model for contaminant and sediment transport via gas ebullition through a sediment cap. *Environmental Engineering Science, 26*(9), 1381–1931.
34. Zheng, L. & Yapa, P.D. (2000). Buoyant velocity of spherical and non-spherical bubbles/ droplets. *Journal of Hydraulic Engineering*, ASCE, 852–855.